ICAS 2021 SHANG HAI
32nd Congress of the International Council of the Aeronautical Sciences
September 6-10, 2021 Pudong Shangri-La, Shanghai, China

REVIEW OF PREDICTIVE METHODS FOR CAPTURING ONSET OF DAMAGE AND INITIAL DELAMINATION IN CARBON FIBRE REINFORCED POLYMER LAMINATES SUBJECT TO IMPACT

Hasan Raza*, Oscar Rodera Garcia+, Kevin Carpenter*, Tuomas Pärnänen+, Jarno Jokinen+
&
Mikko Kanerva+ (mikko.kanerva@tuni.fi) and Javid Bayandor* (bayandor@buffalo.edu)
*CRashworthiness for Aerospace Structures and Hybrids (CRASH) Lab
Department of Mechanical and Aerospace Engineering
University at Buffalo - The State University of New York, NY, USA
+Faculty of Engineering and Natural Sciences, Engineering Materials Science, Tampere University
Tampere, Finland

Abstract

Composite damage modelling and analysis capabilities of Abaqus and LS-Dyna are investigated. A comparison of the modelling methodologies to capture the onset of damage and delamination in the constitutive models used in these codes is presented. A quasi-isotropic carbon fibre reinforced polymer laminate is modelled under a low-energy impact scenario to examine its dynamic response. Hashin, Puck and Cuntze's criteria are implemented for assessing intra-laminar damage in Abaqus in the linear elastic regime without damage evolution, with Virtual Crack Closure Technique being used for inter-laminar failure. In LS-Dyna, the Chang-Chang criteria are used for the intra-lamina failure with damage evolution, whereas delamination is captured using cohesive zone model and Tiebreak contact algorithm. The implementations carried out by both finite element software result in a modelling work well set to analyse and predict the impact response at the initial stages of delamination and damage within the plies. Results obtained using Abaqus demonstrate that the delamination has a higher influence over the failure mechanism of unidirectional plies, as the fracture plane is considered in the failure criteria. On the other hand, LS-Dyna shows a good correlation between the contact force produced from the impact when compared to the force recorded from the experiment. The composite damage criteria used in both finite element codes overall predict stiffer results when compared with the experimental data, however remain in close agreement with each other.

Keywords: ABAQUS, LS-DYNA, CFRP composite, Intra-laminar failure, Delamination

1. Introduction

Carbon fibre reinforced polymers (CFRP) are known for their unique combination of material properties that include high specific stiffness, strength, toughness and improved fatigue performance in the absence of plastic deformation. Due to their remarkable properties, they are finding widespread use in the aerospace industry. CFRP is made up of individual plies that are stacked up with different fibre orientation. This results in three different structural entities, ply, laminate, and the component made from CFRP. The structural response of composite materials can vary between static and dynamic loading conditions. It is associated with intra- and inter-laminar failures. Intra-laminar failure includes both tensile and compressive fibre and matrix damage, whereas inter-laminar failure is primarily associated with delamination of the plies and/or sub-laminates [1-7].

The successful integration of composites in aerospace structures has been brought by improvements in recent computational methods, primarily finite elements (FE) analysis. However, there are difficulties associated with accurately modelling and predicting some of the failure modes, including delamination. Furthermore, there exist several different composite material damage criteria in the literature that have been implemented in commercial FE codes. They include a number of strategies to model interlaminar bonding, such as Virtual Crack Closure Techniques (VCCT), cohesive zone model and surface-based contact interactions [1-2, 5-6].

This study focuses on investigating some of the analysis capabilities within ABAQUS (Abaqus) and LS-DYNA (LS-Dyna), two commercially available FE software, for composite damage modelling

methodologies and their comparisons. Modelling in Abaqus (Dassault Systems) includes the use of three most applied failure criteria referenced in World-Wide Failure Exercise (WWFE) [8], whereas modelling in LS-Dyna (LSTC) focuses on its enhanced composite damage material model. These implementations aim to complement different modelling tools for the analysis of complex failure mechanisms that occur during low-velocity impacts. In addition, delamination initiation is modelled using different techniques offered by Abaqus and LS-Dyna.

2. Experimental Set-up

2.1 Materials and laminate

The CFRP material selected for conducting the tests is AS4/3501-6 UD (Hexcel) unidirectional prepreg. It is stacked to form a quasi-isotropic laminate with a lay-up of [0/45/-45/90]SE and a thickness of 1.12 mm. Each lamina has a square shape of 58.1 × 58.1 mm^2. Figure 1 shows the dimensions of the specimen and the impactor.

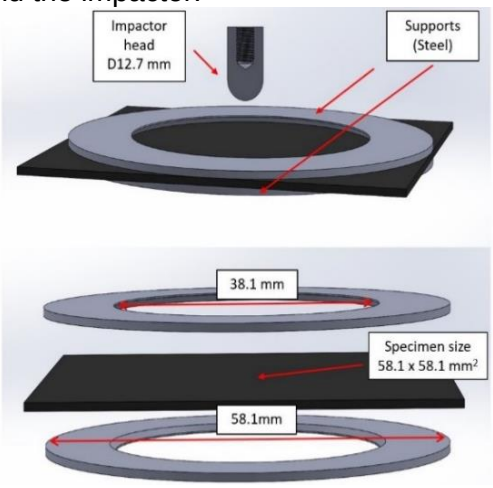

Figure 1 - The dimensions of the specimen, impactor head, and supporting fixture during testing

2.2 Test methods

Calibration data for further modelling work is collected by means of a quasi-static indentation test. The target force is 83 N (weight of the indenter) that induces an elastic response by the laminate specimens. The fixture for the specimen has a circular test area with a diameter of 38.1 mm. Collecting and analysing deformation data is made possible through using Digital Image Correlation (DIC). Two Photron SA-X2 high-speed cameras are used for recording the data, as shown in Fig. 2. DIC provides two-dimensional fields of strain and displacement at the bottom surface ply of the laminate specimen.

The impact tests are conducted in compliance with the ASTM D5628-10 standard [9]. An impact mass (comprising impactor and carriage) is set at a height corresponding to the impact energy of 5 J. The impactor has a hemispherical head with a diameter of 12.7 mm, made of steel (42CrMo4-QT). The total mass of the impactor and carriage is 2.87 kg.

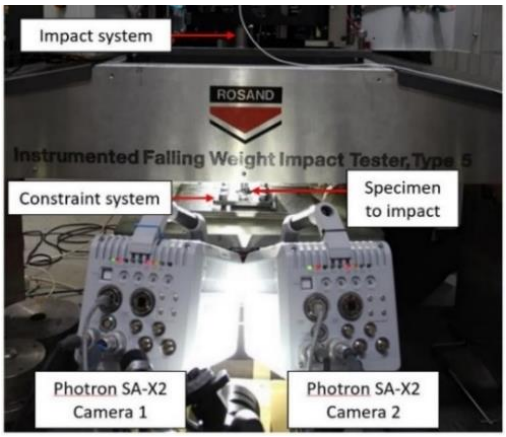

Figure 2. DIC cameras arranged for monitoring the specimen during impact testing

3. Modelling Methodology

3.1 Target modelling in Abaqus

The FE modelling for simulating the indentation test is based on a transversally elastic constitutive model with the elastic constants at the ply level. The simulation is run by using the default methods of Abaqus/Standard.

According to the capabilities offered by Abaqus/Explicit and user subroutine VUMAT, different failure criteria are implemented (Hashin, Puck and Cuntze's). The process for assessing the onset of impact considers two failure paths, ply level failure and delamination occurring between the plies. VCCT is used by means of contact interactions. The analysis is then carried out in the linear-elastic regime with activation (value ≥ 1) of the yielding functions of the criteria as well as the delamination up to its initiation point. Transversally elastic constitutive models are hence implemented in this analysis. Special interest is given to the analysis of the failure at the ply level in the presence of delamination.

3.1.1 Intra-laminar failure

The criteria used in Abaqus are strength-based failure methods, which define activation functions for each of the failure models involved, including fibre, matrix and loading directions. No dissipation of energy occurs by these criteria. Instead, the functions account for the activation of the yielding functions (> 1) describing the failure 'density' based on the effective (undamaged) stress field. These predictions are set to reproduce the impact test up to the point where delamination starts to grow at a pre-existing crack in the 7th interface of the laminate.

Hashin, Puck and Cuntze's criteria are used for the analysis of the intra-laminar failure [8]. These criteria allow for predicting the failure mechanisms caused by two main modes: Fibre Failure (FF) and Inter-fibre Failure (IFF). They have been continuously developed since 1980 when Hashin established his first approach [10]. The criteria by Puck [11] and Cuntze [12] are more recent, where effort is dedicated to improving the IFF mode. IFF is important for the current study because it typically appears as part of bending events [11]. The formulation related to this failure mode based on each criterion is given in the appendix. For fibre failure mode, the three criteria present the same functions, except for the tensile direction. Hashin's criterion is based on the modifications of the Mohr/Coulomb theory through the quadratic functions, as defined in Eqs. (A.1) and (A.2), for the IFF mode.

Puck's criterion, described in Eqs. (A.3) to (A.7b), improves the IFF mode by calculating it as a function of so-called 'action plane stresses' ($\sigma_n, \tau_{nt}, \tau_{nl}$). The common action plane defines the angle of the fracture, shown in Eqs. (A.3) and (A.4). Unlike Hashin's criterion, Puck's is not defined with a fixed angle. The fracture angle is calculated by means of an iterative process related to the IFF functions between -90˚ and 90˚ that maximizes the IFF mode [11].

Cuntze's criterion and its functions, given by Eqs. (A.8) to (A.17), are focused on defining only one global failure model associated with one basic 'strength' [12]. For that, a similar division of the failure functions has been created using the FF and IFF modes, where each failure mode represents a portion of the load-carrying capacity of the material. This capacity and division are quantifying the 'risk' of fracture in each direction, as highlighted in Eqs. (A.8) and (A.9), and the risk in the global failure, calculated from Eq. (A.15) [12].

3.1.2 Inter-laminar failure

VCCT is an efficient method for delamination analysis. The theoretical background of the model is based on the work made by Rybicki and Kanninen [13]. The method has been implemented in several software codes, including Abaqus. VCCT is a fracture mechanics method and requires a pre-existing crack. VCCT evaluates the energy release rate (G) for each fracture mode at the delamination edge (crack-tip) by using nodal displacements and forces. The criticality of the delamination onset is defined with the mixed-mode fracture criterion. The mixed-mode fracture criterion [14] is employed in the current work as:

$$f = (G_{\mathrm{I}}/72)^{0.75} + (G_{\mathrm{II}}/779)^{0.69} \quad (1)$$

Fracture mode III is assumed to be negligible. A high value for G_{IIIC} (10,000 J/m^2) is used in analysis to remove the effects of fracture mode III. VCCT is modelled between the bottom two plies, 7th and 8th. A pre-crack is defined for the interface plane.

3.1.3 Material properties and parameters

The density and elastic constants for the ply are shown in Table 1. The ply strengths are provided in Table 2 and the fracture toughness values are shown in Table 3. Specific parameters of the strength-based failure criteria related to CFRP can be found in Table 4. The properties related to the fibre direction are also given due to the stress effort variable of Cuntze's criterion.

Table 1 - AS4/3501-6 UD laminate ply elastic constants [15]

E_1 (GPa)	$E_2 = E_3$ (GPa)	$\nu_{12} = \nu_{12}$ (-)	ν_{23} (-)	$G_{12} = G_{13}$ (GPa)	G_{23} (GPa)	$Density$ (Kg/mm^3)
142	9.2	0.25	0.29	6.1	3.6	1580

Table 2 - AS4/3501-6 UD laminate strengths [16]

$Hashin's$	X_t	X_c	Y_t	Y_c	S_{12}	S_{13}	S_{23}
$Puck's$	–	–	$R_{\perp}^{+A}$	$2R_{\perp\parallel}^{A}(1+p_{\perp\perp}^{-})$	$R_{\perp\parallel}^{A}$	–	–
$Cuntze's$	$\bar{R}_{\parallel}^{t}$	$\bar{R}_{\parallel}^{c}$	$\bar{R}_{\perp}^{t}$	$\bar{R}_{\perp}^{c}$	$\bar{R}_{\perp\parallel}$	–	–
(MPa)	2172	1558	54	186	87	94	124

Table 3 - Fracture toughness values [17] used in the study

G_{Ic} (J/m^2)	G_{IIc} (J/m^2)	$power\_I$ $(-)$	$power\_II$ $(-)$
72	779	0.75	0.69

Table 4 - Criteria parameters as applied in the study [12]

$Puck's$	$p_{\perp\parallel}^{-} = 0.25$ $p_{\perp\parallel}^{+} = 0.3$	$\frac{p_{\perp\psi}^{-}}{R_{\perp\psi}^{A}} = \frac{p_{\perp\perp}^{-}}{R_{\perp\perp}^{A}} = \frac{p_{\perp\parallel}^{-}}{R_{\perp\parallel}^{A}}$
$Cuntze's$	$0.05 < b_{\perp\parallel} < 0.15$ $1.0 < b_{\perp}^{\tau} < 1.6$ $0 < b_{\parallel\perp}^{\tau} < 0.4$	

1.1.1 FE model of the test specimen and fixture

The models for the indentation and impact tests are constructed in such a way that they are capable of reproducing simulations of indentation (static, implicit) and impact (dynamic, explicit) tests. The size of the FE laminate model is 58.1 × 58.1 mm^2 with a thickness of 1.12 mm as shown in Fig. 3. The laminate mesh is defined with three-dimensional (3-D) hexahedral continuum solid elements with eight nodes and reduced integration (C3D8R).

The mesh at the edge of the plate is defined with a size of 3 mm to obtain a uniform shape at the areas outside of the impact zone. The impact zone (i.e. test area) is constructed with element sizes varying from 1 mm (the outer circle) to 0.3 mm (the inner circle). The central zone of the model presents a refined regular mesh size of 0.3 mm x 0.3 mm, which underlines the size of the intended pre-crack for VCCT. Only one pre-existing crack flaw (in-plane) is modelled between the 7th and 8th plies near the bottom of the laminate. The mesh is designed according to the pre-defined crack at the interface. Transversally isotropic elastic material model is used for the specimen.

The impactor and indenter are modelled as a rigid body using 3-D rigid elements (R3D4) with the mass centre and the radius of the actual instrumented impactor used in the experiment. The contact during the impact occurs between the impactor and the first ply of the laminate. The impact is governed by normal and tangential constraints established with a friction coefficient of 0.3 (steel-composite) in the tangential direction.

The motion of the impactor and the boundary conditions are applied at reference points. All the degrees of freedom (DoF) are fixed, except the out-of-plane direction. For the modelled specimen, the displacements are fixed at the area outside of the test region and at both sides of the laminate to simulate the pressure applied by the fixture.

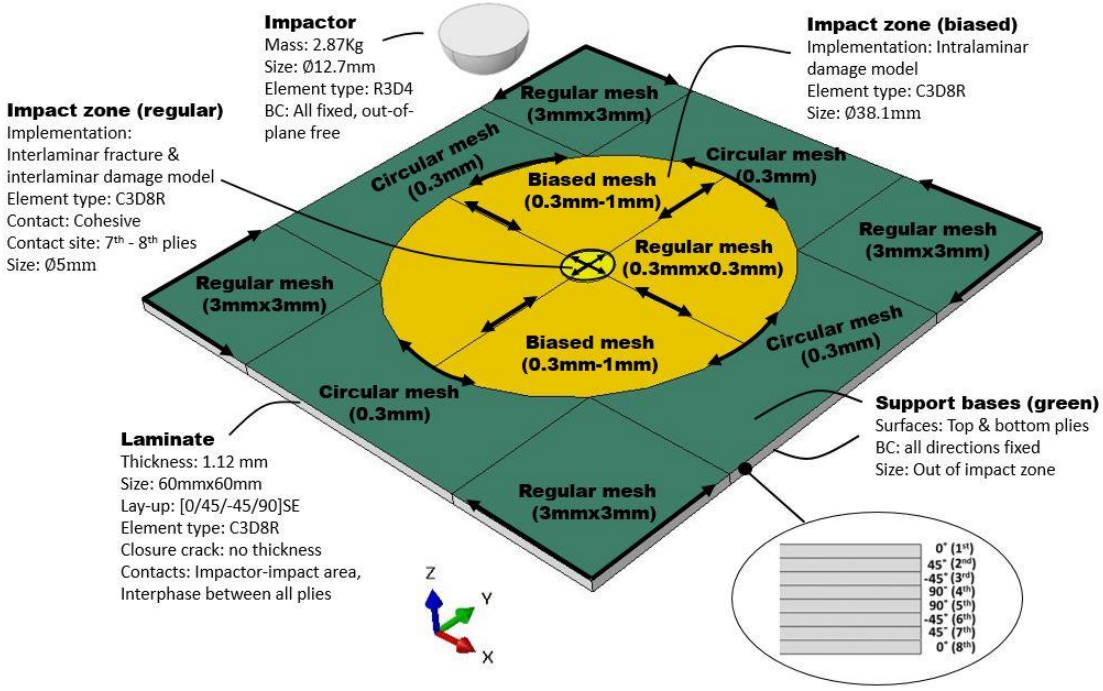

Figure 3 - FE model of the specimen and the in-plane mesh

1.2 Target modelling in LS-Dyna

The constitutive model for simulating the indentation in LS-Dyna is the same as those used in Abaqus: an orthotropic elastic material model with ply and stiffness properties from Tables 1 and 2. The impact test in LS-Dyna is modelled using an enhanced composite damage material model with incorporated damage evolution [18, 22]. Delamination is modelled using two different methods, cohesive zone model with decohesion elements and Tiebreak contact algorithm with contact interaction. The performance of both methods is separately determined using the full model. Special attention is paid to the analysis of the ply failure when delamination exists within the laminate.

1.2.1 Intra-laminar failure

In LS-Dyna, MAT54 material model is used to model the orthotopic unidirectional laminate. The stress-strain behaviour of the material in the elastic region is assessed by [20]:

$$\varepsilon_1 = \frac{1}{E_1}(\sigma_1 - v_{12}\sigma_2) \qquad \varepsilon_2 = \frac{1}{E_2}(\sigma_2 - v_{21}\sigma_1) \qquad 2\varepsilon_{12} = \frac{1}{G_{12}}\tau_{12} + \alpha{\tau_{12}}^3 \qquad (2)$$

where direction-1 indicates the fibre axial direction, direction-2 indicates the matrix transverse direction, and direction-12 indicates the shear direction. Here, α is an input parameter accounting for the nonlinear shear stress term, which must be calibrated whenever shear is present.

Chang-Chang composite damage model [18], as shown in Eqs. (A.18) to (A.21), is used within MAT54 beyond the elastic region. It is an updated form of Hashin's comprehensive composite damage model [19]. The model assumes that unidirectional CFRP behaves transversely isotropic in the fibre direction. It includes a mode mixity term, also known as the shear stress weighing factor, β, which allows interaction between shear and normal failure modes. Setting β to 0 initiates Hashin failure criteria, whereas setting it to 1 executes maximum stress failure criteria [20]. This damage model analytically computes the stresses and damage progression of the fibre and matrix separately to determine the condition of an individual ply.

The Chang-Chang composite damage criteria within MAT54 material model in LS-Dyna assumes a linear elastic orthotropic ply level response until failure, without pre- or post-peak softening. It contains a set of non-physical input parameters which determines the element failure and can be divided into three categories: erosion, crashfront softening factors and parameters describing the material behaviour after failure initiation [21]. For solid elements, an element is deleted when its single

integration point has met the failure criteria. Elements with shared nodes with deleted element become crashfront elements which can have their strengths reduced by varying the non-physical SOFT input parameters. Failed ply can still carry a significant amount of stress and energy, and only once it reaches failure using one of the non-physical input parameters or an effective failure strain, the stresses are reduced to zero and the element is deleted [22]. For this study, the built-in default YCFAC strength reduction factor for compressive fibre strength after matrix failure is used to degrade the fibre strengths of the plies if compressive matrix failure would take place [22]. This parameter simulates damage caused to the fibres from failed matrix [20]. Additionally, the built-in default SOFT material strength reduction parameter is used to reduce the strengths of the elements ahead of the crashfront [22]. It is used to degrade the strengths of the surrounding elements to simulate the damage propagation from the crashfront [20]. None of the failure input parameters are used nor any effective failure strain is defined in order to keep elements from deletion.

3.2.2 Inter-laminar failure

3.2.2.1 Cohesive zone modelling

Cohesive zone model (CZM) [22,23] is based on the fracture model originally proposed by Dugdale [30] and Barenblatt [31,39]. An alternative to the VCCT, it is one of the most widely used approaches to investigate interface bonding failure. It assumes a cohesive damage zone that develops near the crack tip and uses strain energy release rates, G, during the formation of fracture to predict delamination [38]. Hence, CZM is governed by the properties of the material, crack initiation condition and a crack evolution function, where it relates the surface loads in normal and shear direction, σ, to the displacement. Crack initiation takes place when the model reaches maximum interface strength, σ^0, that is the maximum load on stress-displacement relation [24,38].

There exist many linear and non-linear constitutive failure damage formulations for defining the cohesive law. The law used in this study is governed by a bilinear stress-displacement relation as well as mixed-mode to represent the interactions of mode I, mode II and mode III separation. Figure 4 shows the bilinear stress-displacement relation used in this study [25,38]. The area under the stress-displacement relation is equal to the energy release rate, G, or the fracture toughness G_c, that is the critical value of G for delamination growth [26,39]. In LS-Dyna, energy release rates are assigned for both mode I and mode II. Mode III is assumed to be nearly identical to mode II separation. This allows the cohesive model to utilize mixed mode capability which combines the energy release rate. This is used in conjunction with a damage formulation (progressive softening) where mixed-mode displacement for total failure is computed using either Power law or Benzeggagh-Kenane (B-K) law [27]. The interface bond softening happens when the separation and sliding between the plies exceeds the softening strain, δ^0. Once the failure strain, δ^F, is reached, the interface bond fails and delamination occurs [38]. The formulation for Power and B-K law implemented in LS-Dyna can be found in [22].

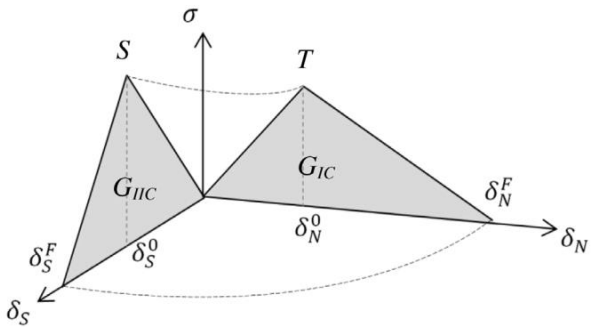

Figure 4 - Bilinear stress-displacement [22,38].

The slope of the bilinear stress-displacement before damage initiation, *K*, is known as the interface stiffness or penalty stiffness as it is referred to in LS-Dyna. Turon et al. [24] formulated that the effective elastic properties of the composite laminate are not affected by the cohesive surface properties whenever $E_3 \ll Kt$, that is:

$$K = \frac{\alpha E_3}{t} \tag{3}$$

where E_3 is the through-thickness Young's modulus of the material, which for a transversely isotropic material is $E_3 = E_2$ and t is the sub-laminate thickness. α is a parameter that is recommended to be much larger than 1. Values of α are recommended to be greater than 50 [24].

The crack propagates when the energy release rates reach their critical values G_c, that is their fracture toughness [24]. The distance from the crack tip to the point where the maximum stress (cohesive traction) is achieved is referred to as the length of the cohesive zone, l_{cz}. Several different models have been proposed to estimate the cohesive zone length [28-35]. All of these proposed models have the form:

$$l_{cz} = ME\frac{G_c}{(\sigma^0)^2} \tag{4}$$

where E is the Young's modulus of the laminate and M is a parameter that depends on the different cohesive zone length models. This study uses the Rice [32] and Falk et al. [33] recommended parameter defining .the cohesive zone length. In terms of LS-Dyna parameters, the cohesive zone lengths can be defined for both mode I and mode II as:

$$l_{cz,I} = ME\frac{G_{Ic}}{(T)^2} \quad \text{and} \quad l_{cz,II} = ME\frac{G_{IIc}}{(S)^2} \tag{5}$$

where *T* and *S* are the normal and shear peak load input values. For mixed-mode, the cohesive zone length must satisfy the condition:

$$l_e \leq \frac{l_{cz,I}}{N_e} \quad \text{and} \quad l_e \leq \frac{l_{cz,II}}{N_e} \tag{6}$$

where N_e is the number of elements in the cohesive zone and l_e is the mesh size used in the direction of crack propagation [24, 35]. If the cohesive zone is not discretized by enough elements, then the distribution of load ahead of the crack is not represented correctly in FEM. Therefore, Turon et al. [24] suggest using a minimum of 3 elements in the cohesive zone to predict the propagation of delamination. However, such fine mesh requirements can make structural analysis computationally expensive and therefore not feasible for some studies [35]. It can be seen from Eq. (6) that the cohesive zone length is inversely proportional to the square of the interface peak loads. The length of the cohesive zone can therefore be theoretically lengthened to ensure that they span enough elements of the given size. Using this methodology, we can obtain the required normal and shear peak loads that would allow us to use an appropriate cohesive zone length without making the mesh overly fine [24,35]:

$$T^0 = \sqrt{\frac{9\pi E G_{Ic}}{32 N_e l_e}} \quad \text{and} \quad S^0 = \sqrt{\frac{9\pi E G_{IIc}}{32 N_e l_e}} \tag{7}$$

and the normal and shear peak loads to be used in the model can be selected based on the criteria:

$$\bar{T} = Min\{T^0, T\} \quad \text{and} \quad \bar{S} = Min\{S^0, S\} \tag{8}$$

3.2.2.2 Tiebreak contact

An alternative to the cohesive zone model technique is the Tiebreak contact algorithm in LS-Dyna that uses a segment-based approach to model cohesive interaction between the plies or laminates. By implementing the Dycoss Discrete Crack Method [36] within the Tiebreak algorithm, a bilinear stress-displacement relation can be used similar to the cohesive law explained in section 3.2.1. This contact algorithm essentially models a theoretical interlaminar bonding based on the normal and shear peak stress. This allows the delamination to propagate from the initiation zone based on mixed-mode, which combines the crack opening damage (mode I) and in-plane shear damage (mode II). This is used in conjunction with a damage formulation where mixed-mode displacement for total failure is computed using either Power Law or Benzeggagh-Kenane's [27]. An advantage of this method is that it does not require any additional layer of elements to be modelled or defined at the interface as it uses a segment-based approach, where the faces of the ply elements are bonded. Figure 5 shows a comparison between the cohesive zone model and Tiebreak contact.

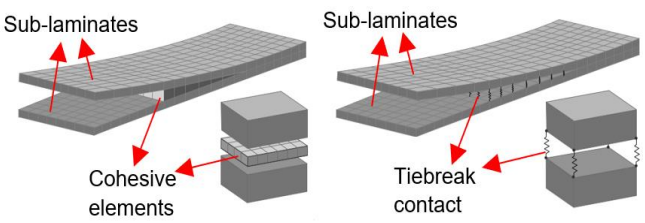

Figure 5 - Cohesive elements and Tiebreak contact comparison [37]

3.2.3 Quasi-static and dynamic model

The FE models for both indentation and impact tests are set up similarly to Abaqus where similar mesh and boundary conditions are applied. Figure 6 shows the boundary condition that is applied to the laminate for both tests. The impactor is modelled as a rigid body using 3-D solid elements that are assigned rigid properties. For the indentation test, a more uniform mesh is used for the impact zone. Displacements are fixed on the area outside of the impact zone at both sides of the laminate with the aim of simulating the supports pressure. The plies are modelled using fully integrated quadratic eight nodes solid element with nodal rotations. In total eight plies are modelled representing the stacking sequence of [0/45/-45/90]SE. Figure 7 shows the ply layup of the FE model.

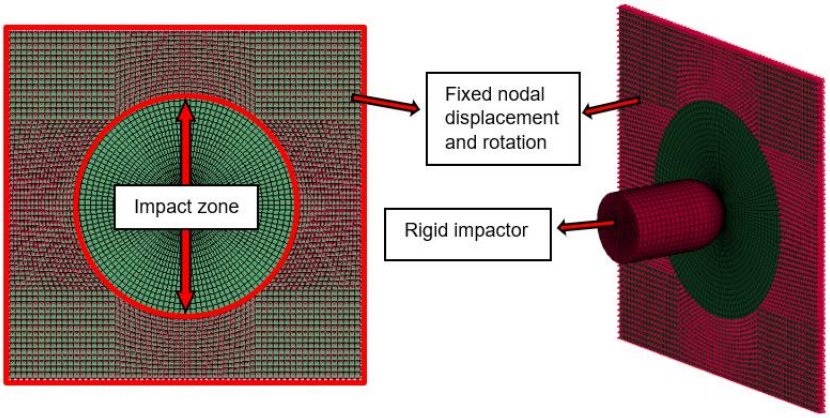

Figure 6 - Boundary conditions of the model

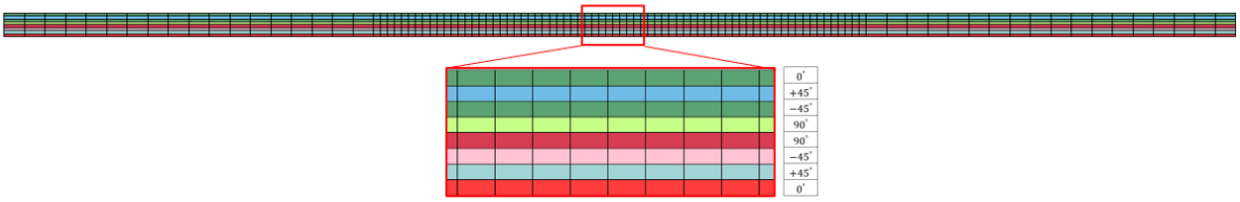

Figure 7 – Laminate layup

A surface to surface tied contact is used to model the interlaminar bonding in the indentation test as well as the impact test with the exception being between 7th and 8th plies, where delamination is modelled using cohesive zone model and Tiebreak contact. This approach is adopted because the primary focus of this study is to model damage onset, which initiates in the bottom plies in low energy deformation scenarios.

4. Results

4.1 Indentation test

For the case of the static test simulation (indentation), the results obtained from DIC are compared with the FE results from the two constitutive models employed in this work (Abaqus and LS-Dyna). The displacement field is shown in Fig. 8, while the strain field is depicted in Fig. 9, both at the bottom ply (8th ply) of the laminate. DIC outputs a displacement field based on a stepped distribution with its maximum value at the central region of the bottom ply. The results are in close agreement with the experimental finding. The displacement field follows the general trend where maximum displacement is found near the test area. The displacement in the ply radiates outwards as expected and seen from the experimental measurements. The magnitude of the displacement decreases as we move further away from the central impact region. FE results indicate values in the negative z-direction, which represents the direction in which the load is applied. Using both Abaqus and LS-Dyna, the maximum displacement is found to be at the centre of the impact region, where it reaches a value of 0.25 mm, consistent with the DIC results.

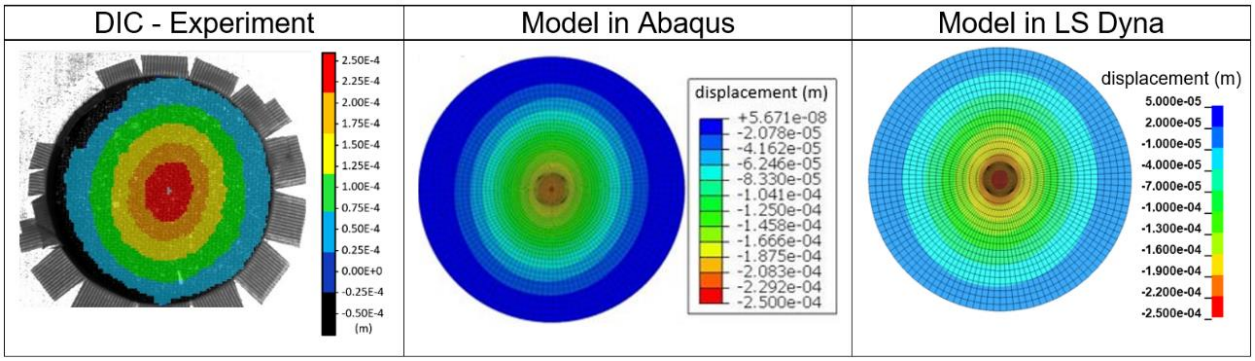

Figure 8. Displacement fields – DIC data compared to FE simulations

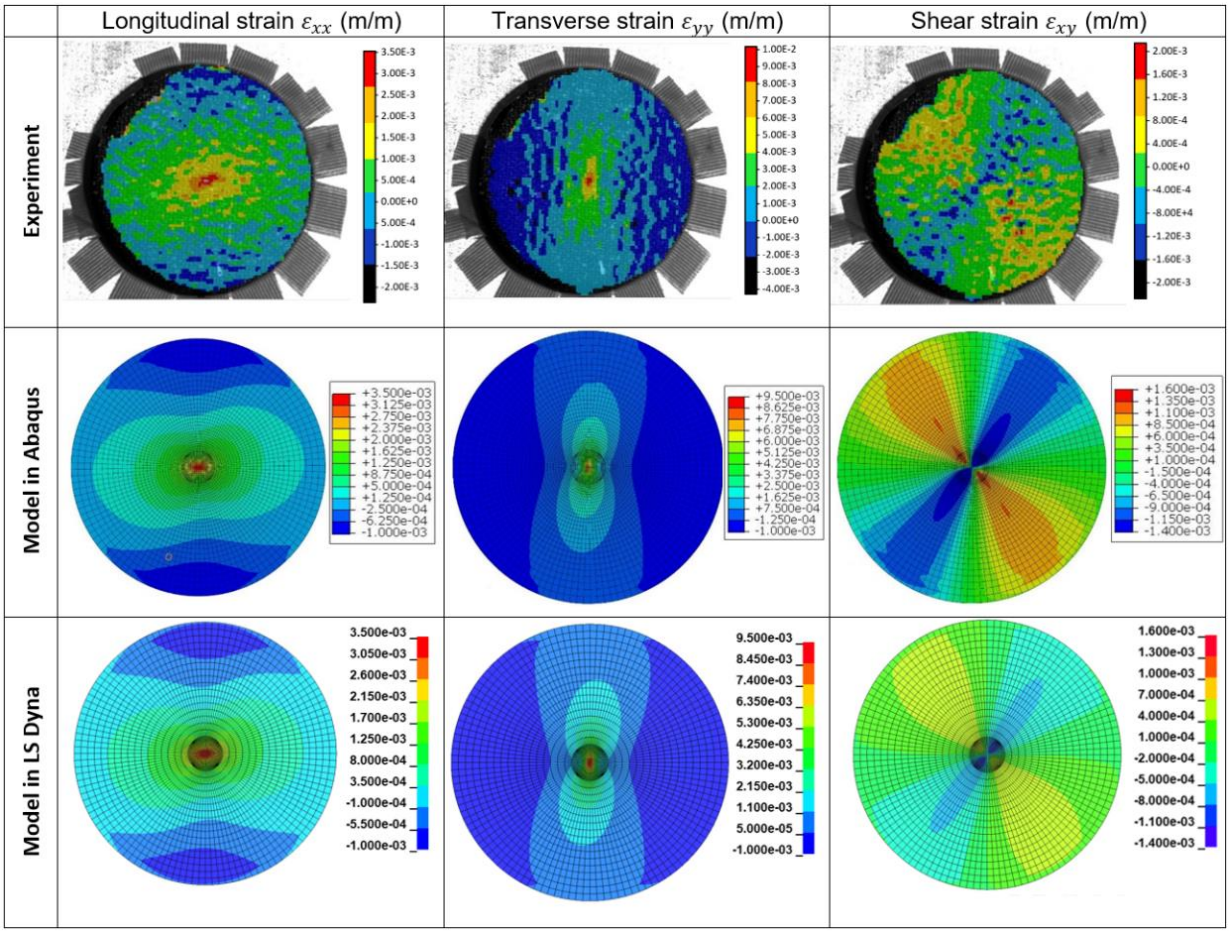

Figure 9 - Strain fields – DIC data compared to FE simulations

The DIC based strain field is compared for the three in-plane directions at the bottom ply of the laminate, namely, longitudinal, transverse and shear axes. FE results show a similar trend for all three in-plane directions. For Longitudinal strain, ε_{xx}, maximum strain is found to be at the centre where it reaches 0.0035 m/m (for both constitutive models). The minimum is seen at the outermost region of the impact area where values range from 0.0001 to -0.001 m/m. For the transverse shear strain, ε_{yy}, the maximum strain value in the transverse direction is found to be at the centre of the impact region where the value rises to 0.0095, whereas the minimum value is around the outer region where it reaches -0.001. These are values in close proximity to the experimental maximum and minimum values. Shear strain, ε_{xy}, results are found to be close to the experimental results, however, it can be seen that they vary slightly between the two constitutive models, with Abaqus results being slightly stiffer. Nonetheless, the results are in the acceptable range where maximum strain of around 0.0016 occurs at the outer regions of the impact area and minimum strain of around - 0.0014 at the centre region.

Figures 10(a) and 10(b) show the overall deflection in the XZ and YZ planes. The results obtained using the constitutive model of Abaqus and LS-Dyna match well with experimental data in fibre direction (0˚ ply). It can be seen that FE results obtained for the XZ direction are close to the experimental data in terms of both the values and curve shape, however for the YZ direction, only in terms of the curve shapes. This could be due to the fact that the DIC data for the YZ direction have a smaller regression error ($R^2 = 0.97$) than in the XZ direction. This deviation might be a consequence of non-central impacting or asymmetry of the laminate.

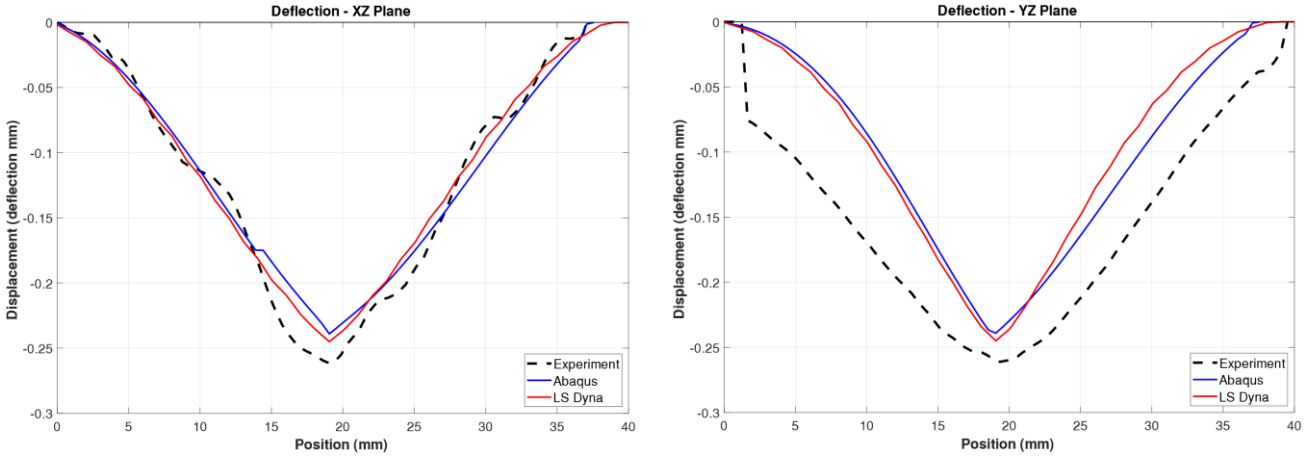

(a) (b)

Figure 10 – Comparison for the XZ (a) and YZ (b) deflection for the laminate

Overall, both constitutive models capture the deflection well in YZ and XZ directions. Table 5 provides the maximum displacements found using the experiment as well as the constitutive models. The maximum displacements from the experiment are approximately 0.26 mm in both XZ and YZ directions. Comparing the FE results, the constitutive models offer equivalent performance with less than 9% error. Their results are consistent with the fact that depending on the mesh size FE models tend to provide stiffer responses.

Table 5 – Maximum displacement comparison

	XZ	Percent Error	YZ	Percent Error
Experiment	0.2615 mm	-	0.2611 mm	-
Abaqus Model	0.2391 mm	8.57 %	0.2391 mm	8.43 %
LS-Dyna Model	0.2450 mm	6.31 %	0.2450 mm	6.17 %

4.2 Abaqus impact model

For the explicit analysis in Abaqus, the initiation of delamination is modelled at the 7th interface. Figure 11 shows the schematic where the pre-crack is located.

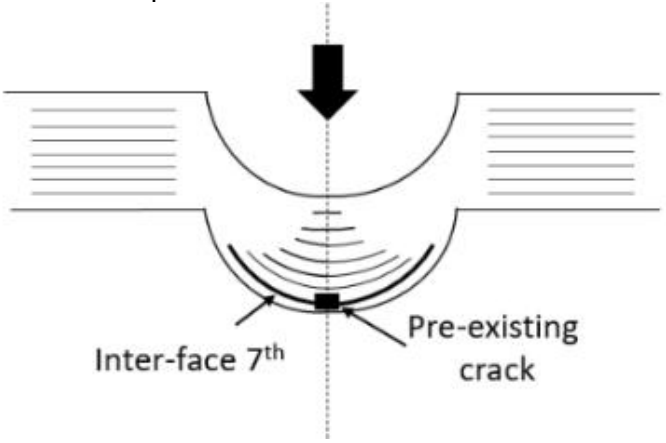

Figure 11 – Scheme of pre-crack

Figure 12, the activation functions (IFF mode) of the three failure criteria through the thickness and with the pre-crack at the 7th ply interface. The tensile (membrane) response acts at the bottom part and compression at the top of the laminate due to bending. Figure 13 shows the von Mises stress field. Figure 14 and 15 shows in details the von Mises stress and the failure status (inter- and intra-laminar) of the bottom part of the ply 7th, respectively. Results are shown at the point when delamination starts to evolve, indicated with the IFF mode values at the ply. In terms of the stresses and failure values, the simulated prediction is highlighted by the 48 elements that are used for reporting the performances, shown in Tables 6, 7, 8, 9 and 10. The simulation is conducted for the model without the pre-crack at the 7th interface as well.

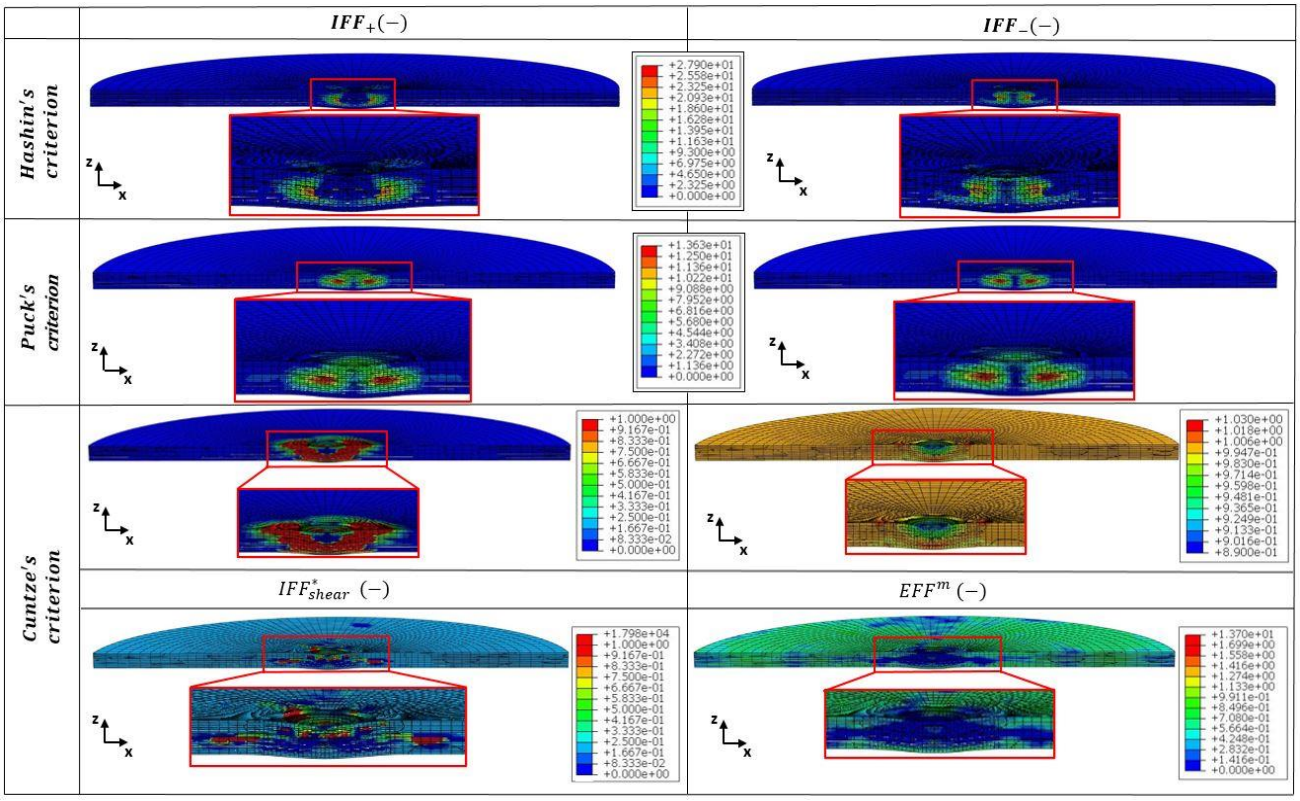

Figure 12 - Stress and activation functions status through the cross-section of the laminate

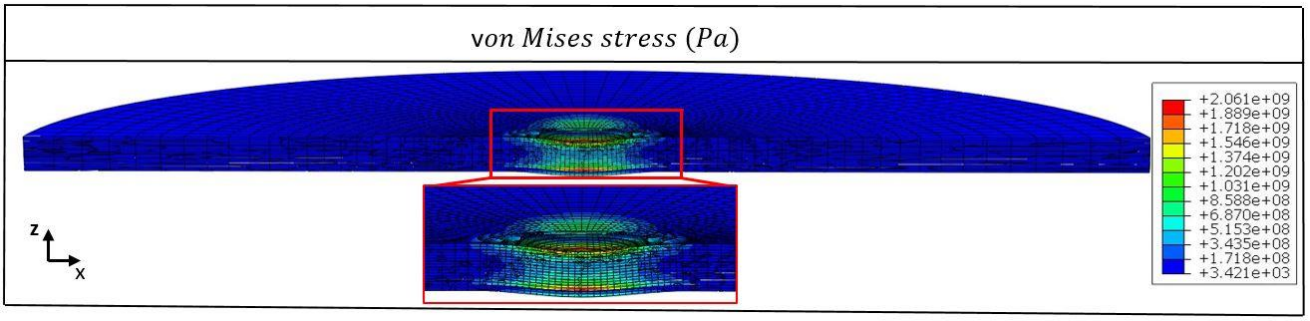

Figure 13 - von Mises stress through the thickness at delamination initiation at the 7th ply interface

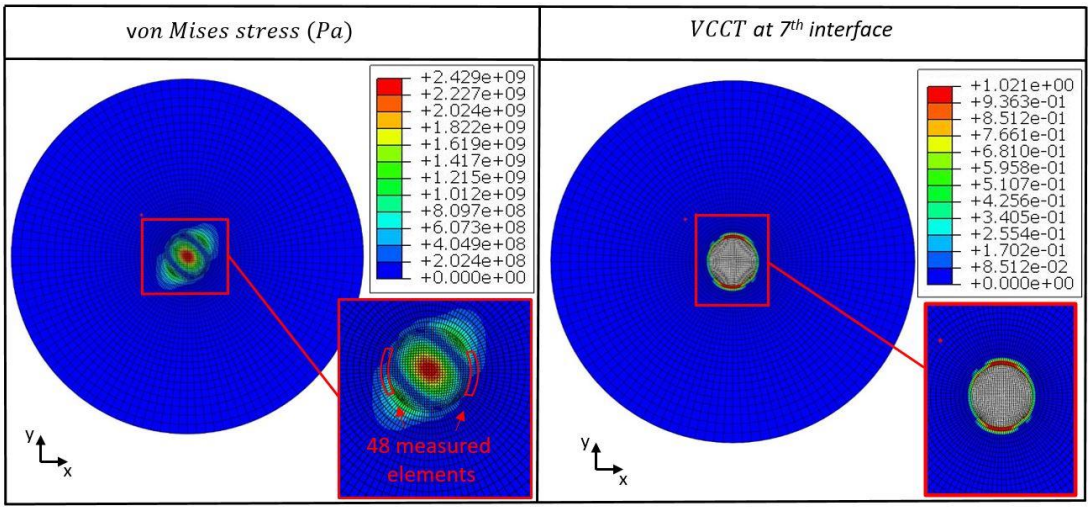

Figure 14 - von Mises stress and VCCT results at the delamination initiation at the 7th ply interface

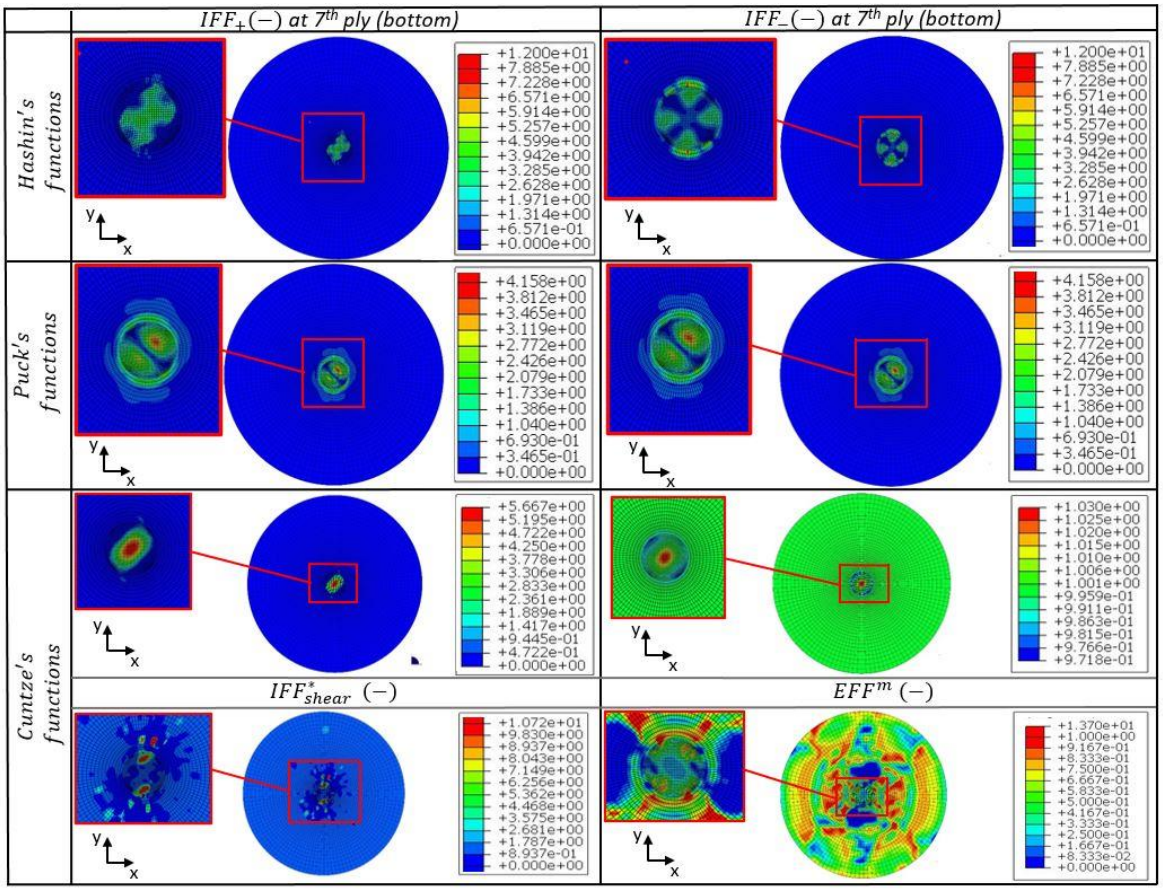

Figure 15 - Comparison of the failure prediction at the delamination initiation at the 7th ply interface

Hashin's criterion, shown in Table 7, presents the highest value for the compressive mode, making it the most conservative with respect to the two other criteria. This is due to the definition of the fracture plane at a 'pre-fixed' angle ($\mathbf{0}$° wrt. thickness direction), on which transverse stresses act. The simulations without pre-crack shows a slight increase in the probability of tensile failure, as well as an abrupt decrease in the compressive failure due to the stress field reduction ($-\mathbf{66.1}\%$).

Table 6 - Averaged values of the von Mises stress of the highlighted elements at the 7th ply interface

48 Elements at 7th interface	Pre-existing crack model	Tie constraint model
$\boldsymbol{\sigma_{VM,max}}$ (*MPa*)	546.453 ± 236.27	185.390 ± 79.341

Table 7 - Averaged values of the IFF mode (Hashin's criterion) of the marked elements

Hashin's failure modes		
48 Elements at 7th interface	Pre-existing crack model	Tie constraint model
$\boldsymbol{IFF_+}(-)$	0.172 ± 0.078	0.191 ± 0.215
$\boldsymbol{IFF\_}(-)$	3.313 ± 1.064	0.217 ± 0.141

Table 8 - Averaged values of the IFF mode (Puck's criterion) of the marked elements

Puck's failure modes		
48 Elements at 7th interface	Pre-existing crack model	Tie constraint model
$\boldsymbol{IFF_+}(-)$ $(\boldsymbol{\theta_{frac}} = \mathbf{55.622}^\circ)$	0.606 ± 0.124	1.088 ± 0.109
$\boldsymbol{IFF\_}(-)$ $(\boldsymbol{\theta_{frac}} = \mathbf{55.622}^\circ)$	0.538 ± 0.129	0.963 ± 0.108

Table 9 - Averaged values of the IFF mode (Cuntze's criterion) of the marked elements

Cuntze's failure modes		
48 Elements at 7th interface	Pre-existing crack model	Tie constraint model
$\boldsymbol{IFF_+}(-)$	0.167 ± 0.049	0.254 ± 0.275
$\boldsymbol{IFF\_}(-)$	0.987 ± 0.003	0.999 ± 0.001
$\boldsymbol{IFF_{shear}}(-)$	2.409 ± 0.737	0.562 ± 0.896
$\boldsymbol{EFF}(-)$	0.194 ± 0.117	0.507 ± 0.32

In the highlighted elements, shown in Fig. 14, Puck's criterion on average results in a fracture plane at 55.52° (wrt. thickness direction). The results with the pre-crack for the compressive mode are found to be lower than Hashin's criterion with pre-crack. Whereas, the results with the pre-crack for the tensile mode are found to be higher than Hashin's criterion with pre-crack. However, without the pre-crack, the IFF values are found to be higher. This solution represents a clear difference in comparison to Hashin's criterion.

The global response ($\boldsymbol{EFF}$) of Cuntze's criterion offers a higher predicted failure value for the case without a pre-existing crack (see Table 9). The local response of this criterion ($\boldsymbol{IFF}$), unlike Puck's, is defined with 'fixed' fracture angles based on experimental results [12]. The IFF1 value is generated by a fracture plane parallel to the fibres ($\mathbf{0}^\circ$ wrt. thickness direction) and it reports a slightly higher value in the simulation without a pre-crack. The IFF3 mode is defined by a fracture plane of 53° [11], which results in a higher value than in the case with a pre-crack. The IFF2 (shear) mode is also represented by a fracture plane parallel to the fibres ($\mathbf{0}^\circ$ wrt. thickness direction), resulting in the highest simulation values with a pre-crack (i.e. higher stress field). However, the failure value reduces drastically for the simulation without a pre-crack (i.e. lower stress field). Therefore, a similar response to that of the Puck's is obtained: an increase in the IFF failure prediction without a pre-crack.

The difference between the results of Hashin's criterion versus Puck's and Cuntze's criteria, for the IFF mode, is essentially due to the definition of the fracture angle. Hashin's criterion results in a higher IFF value in the simulation with an embedded pre-crack (i.e. higher stress field). However, when the stress field reduces, as in the simulation without a pre-crack, the IFF value decreases. This behaviour does not occur in the other two criteria. Although, the two criteria result in an increase in the IFF mode as a consequence of the rise in the failure throughout the UD-plies, rather than the interface, where no delamination takes place (no pre-crack, no VCCT).

Table 10 - Averaged values of FF mode (Hashin, Puck and Cuntze) in marked elements at the 7th ply interface

48 Elements at 7th interface	Pre-existing crack model	Tie constraint model
$\boldsymbol{FF_+}(-)$	0.4085-0.4113	0.0931-0.0253
$\boldsymbol{FF\_}(-)$	0	0

As seen in Table 10, for the common responses, including the fibre failure modes (tension/compression) measured by the three criteria, higher values are obtained at the element level when a pre-crack exists. This is due to the partial lack of load-carrying capacity in the plies in the presence of the pre-existing crack. For the simulations without a pre-crack, FF modes result in values nearing zero. This result does not occur for the global response (EFF) of Cuntze's criterion, as mentioned earlier. For the case of Hashin, the FF tensile mode, defined in Eq. (A.17), results in the same values for pre-crack simulations as those without pre-crack.

4.3 LS-Dyna impact model

Chang-Chang composite damage model is applied to the plies, and delamination is modelled between the 7th and 8th plies to determine the damage onset. Element deletion is not used for this study to obtain an elastic response. A layer of cohesive elements is modelled between bottom plies with a thickness of 0.01 mm. Unlike VCCT, CZM does not require the existence of an initial crack in the structure and therefore is able to represent the complete interlaminar bonding layer. Figure 16(a) shows the delamination initiation. Cohesive elements reaching failure due to the applied load over time are deleted from the cohesive layer thereby representing the crack initiation, highlighting delamination and damage onset. Figure 16(b) shows the subsequent delamination as it propagates.

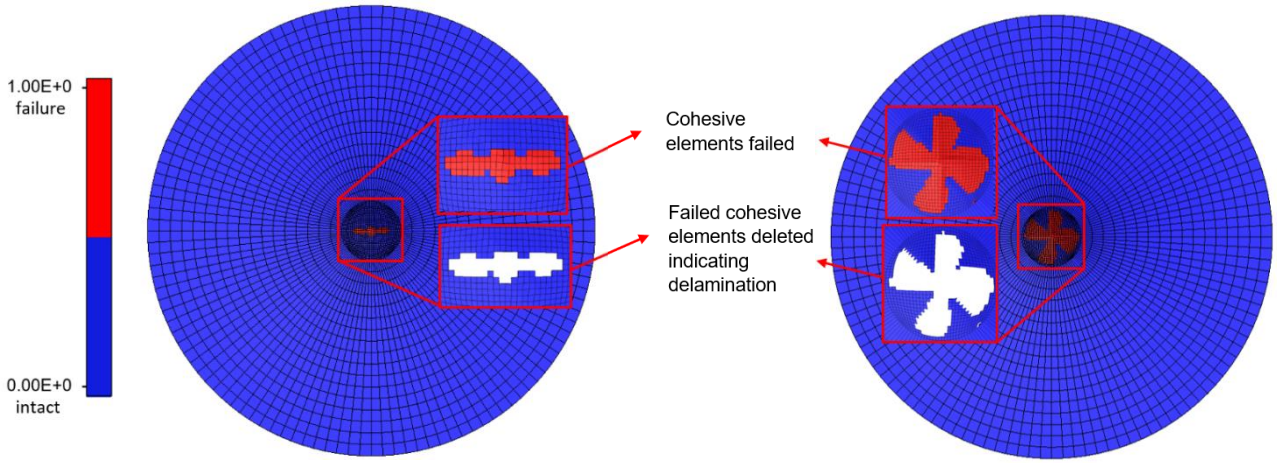

(a) (b)

Figure 16 – (a) Initial delamination at 0.446 *ms* (b) delamination propagation

Figure 17 portrays the fibre and matrix damage at initial delamination for the bottom side of the 7th ply. Damage onset takes place at the centre region as expected where the impactor strikes the laminate. Fibre is shown to be damaged in tension in the $+45^{\circ}$ direction along the fibre orientation. Damage initiates near the centre for the fibre in compression. It can be seen that the 7th ply fibres do not seem to fail from a 5 J impact since no element reaches the failure value of 1. Matrix on the other hand is seen to be both damaged as well as failed in tension near the centre region where the impact primarily takes place. This is expected since matrix is more prone to damage and failure than fibre in general, when the ply is deflected downwards due to an impact load. The matrix further seems to be damaged and failed in compression. The regions where the matrix fails are close to where the delamination initiates.

Figure 18 shows the damage onset through the thickness of the laminate. It can be seen that the fibre damage in tensions starts at the bottom two plies and then propagates upwards. Fibre in compression on the other hand is seen to have failed in some regions in the upper plies as expected. Matrix in tension follows a similar trend where the failure initiates at the bottom plies and propagates upwards. Matrix in compression follows the trend of the fibre in the sense that it fails in the upper plies and gets damaged in the bottom plies.

Figure 19 depicts the comparison of von Mises stresses within the 7th ply between the CZM and Tiebreak constitutive model at initial delamination. It can be seen that the stresses are about the same magnitude and their distribution is almost identical. The cohesive zone model predicts slightly higher stresses in the laminate near the centre region as compared to the Tiebreak model, however, the difference is minimal. The maximum stresses are found to be at similar locations where they reach a

value of about 1.27 GPa. Near the centre region of the impact, the stresses in both models are found to be in the range of 350 – 650 MPa.

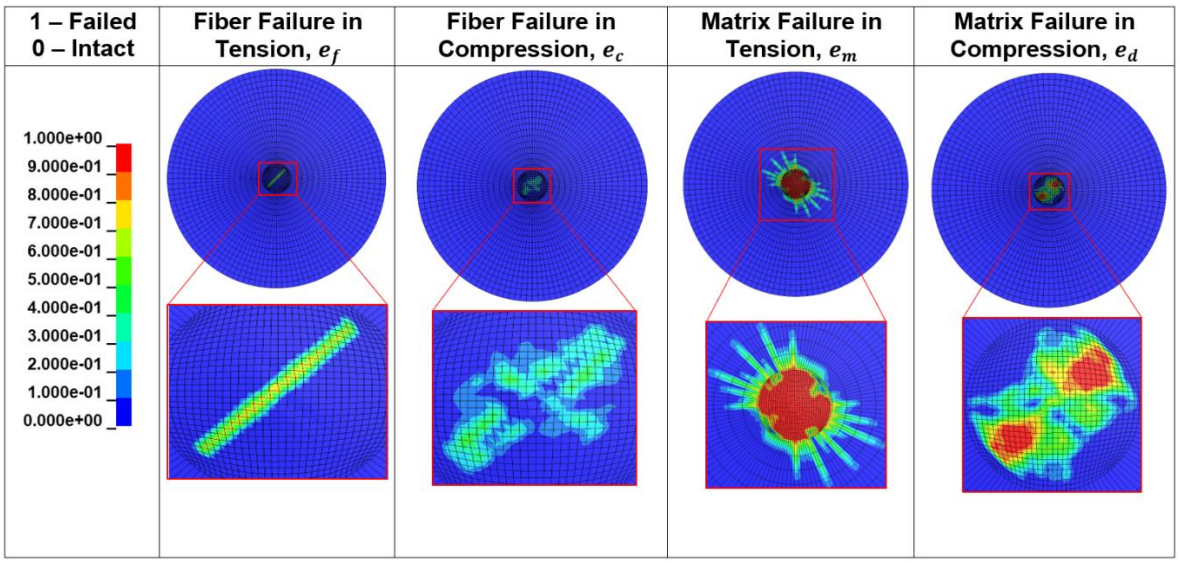

Figure 17 – Damage at the onset of delamination

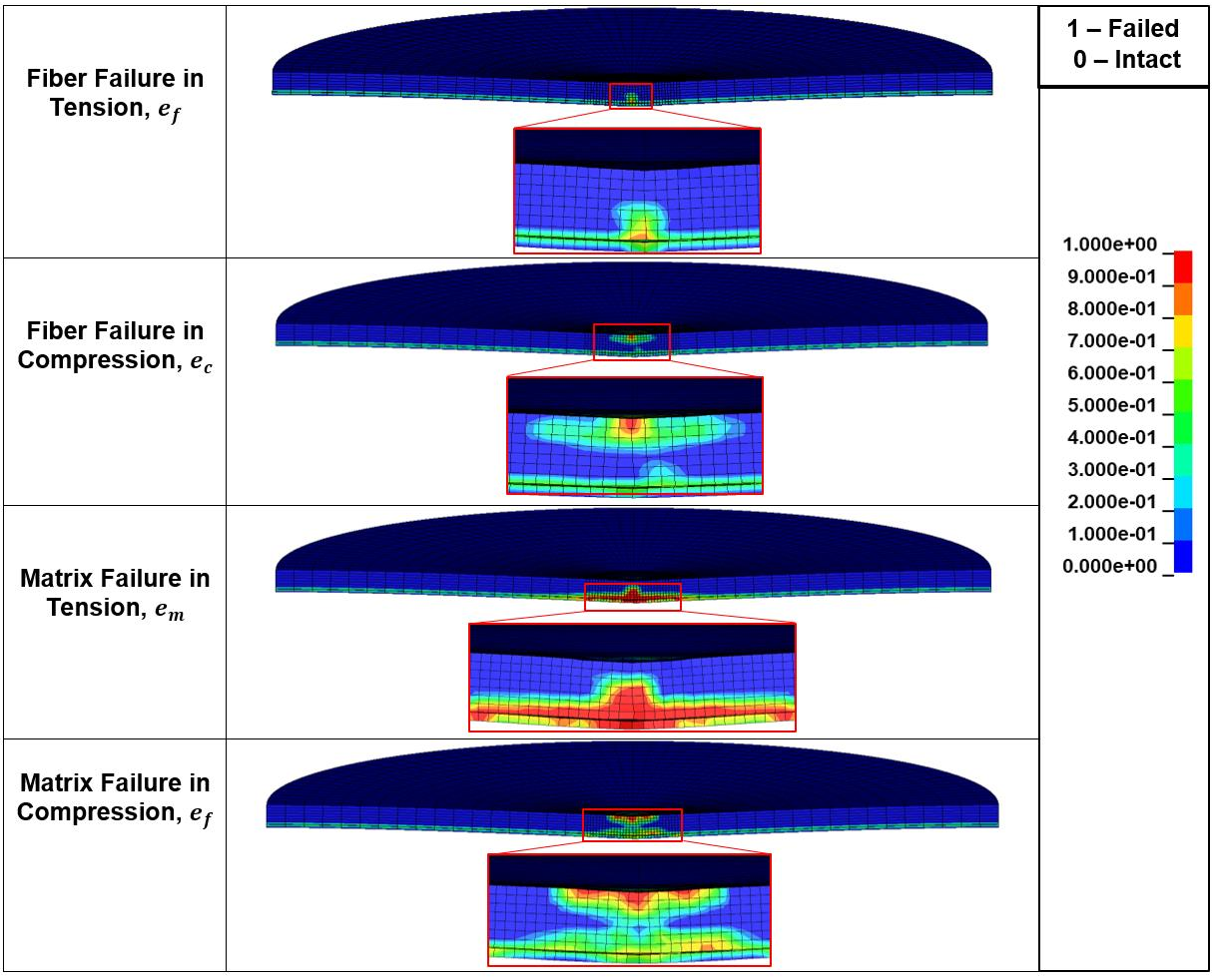

Figure 18 – Damage onset through the thickness of the laminate

Figure 20 shows the force-time history of the CZM and Tiebreak constitutive models in LS-Dyna compared with the experimental data. Initial delamination takes place at 0.446 ms, which is indicated by a dashed vertical line. Both models follow the trend of force-time history well. Large drops in load are seen around 0.43-0.45 ms when initial delamination occurs in both constitutive models. Consequent drops in the load indicate delamination propagation that is seen once the initial crack is formed. The reason for this can be conjectured as follows: since the delamination is not modelled in

all plies and element failure is turned off, the laminate undergoes an elastic response, which in turn results in increased load-bearing capacity of the structure.

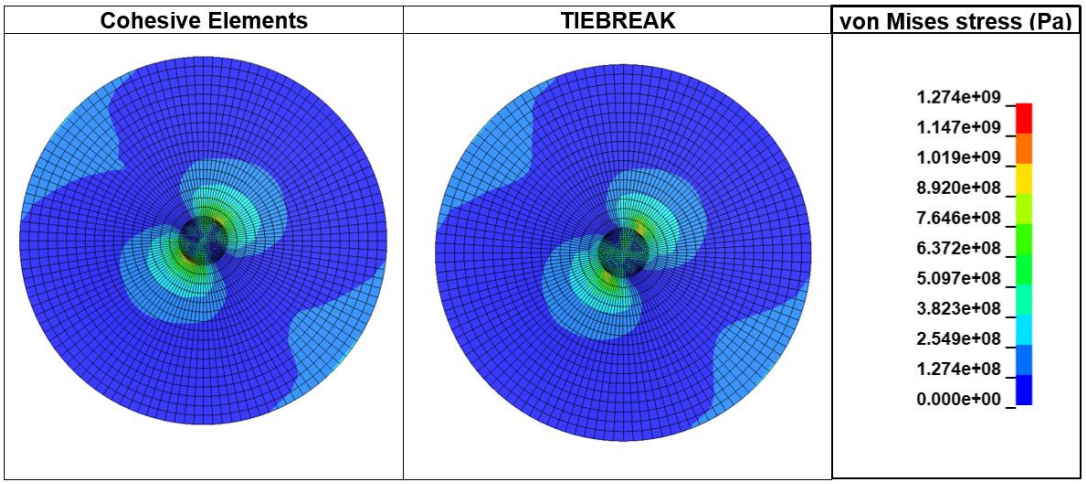

Figure 19 – Stress comparison between CZM & Tiebreak model at the 7th ply at initial delamination

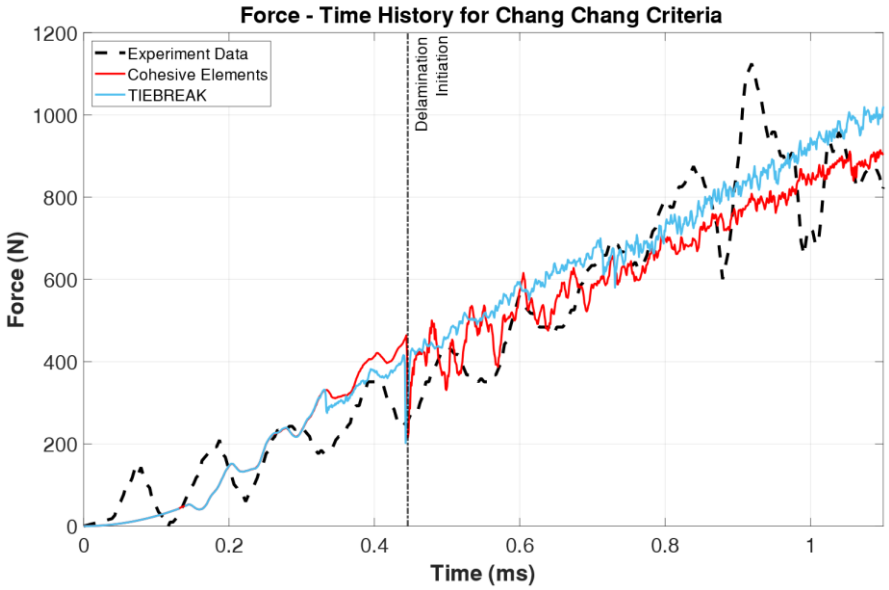

Figure 20 – Force-time comparison of CZM & Tiebreak models in LS-Dyna with experiment

5. Discussions and Conclusion

For the indentation test, the maximum and minimum strain magnitudes of the FE results are within the range of the readings obtained using DIC. Overall, the results from the constitutive models implemented in Abaqus and LS-Dyna compare well with each other and with the experiment as both show a maximum displacement of about 0.25 mm at the centre. As a consequence, it can be assumed that the elastic models are capable of simulating the experimental behaviour of the laminate accurately.

The VCCT simulations carried out using Abaqus result in a stiffer response around the pre-designed inclusion for the cases without a pre-crack. This is due to the way that VCCT contacts are defined: with infinite stiffness. The global response of the laminate therefore is influenced, making the laminate stiffer. Through the implementation of the failure criteria in terms of effective stresses, Abaqus can analyse the influence of a pre-crack in damage evolution cases. The damage footprint can increase in UD-plies where VCCT is not implemented. The user defined subroutine capabilities within Abaqus allow failure criteria that are not otherwise part of its default library to be developed. The implementation of the subroutines for Cuntze and Puck's criteria allowed the characterization of the global response of the laminate and the determination of the fracture angle. VCCT used in conjunction with the subroutines allowed to investigate the influence of delamination.

The models simulated using LS-Dyna are able to predict the damage onset, as well as delamination well. Their stiffer response as compared to the experimental results of force-time history could be because the elements are not deleted, and hence are able to carry a significant amount of stress and energy. Initial delamination is captured well using cohesive elements, showing their capabilities to both accurately predict as well as visualize the spread of delamination effectively. Comparing CZM with Tiebreak, it can be seen that von Mises stresses in both methods are about the same magnitude and their distributions are almost identical. Comparing the force-time history curves of the two with the experimental results, it is observed that both curves follow the overall trend well and predict the force magnitude with good correlation. Furthermore, delamination initiation occurs at the same instant for both models, highlighting that each method is capable of predicting delamination occurrence competitively. Tiebreak model is found to be more computationally expeditious than CZM.

Comparing the results between Abaqus and LS-Dyna, it is observed that the constitutive models are able to simulate damage distribution and delamination initiation in similar regimes. As it can be noticed from the force-time history curves, the delamination phenomena without degradation in the UD-plies (Abaqus) occurs much earlier than the models with damage evolution (LS Dyna). This is due to the higher load-bearing capacity of the UD-plies at linear-elastic regime, making the response stiffer at the interface. Additionally, the pre-crack modelled using VCCT makes delamination perform faster as a consequence to the zero strength in that zone. The experimental response of the laminate up to the delamination initiation point can further be predicted well using LS-Dyna's constitutive model. As design tools, both LS-Dyna, with its composite damage and delamination features, and Abaqus, with its user defined elastic model capabilities, allow for a better understanding of the intricate dynamic performance of structures subject to low velocity impact by accurately capturing the onset of damage and mechanisms of its progressive failure.

6. Contact Author Email Address

Corresponding authors:
Mikko Kanerva; mikko.kanerva@tuni.fi and Javid Bayandor; bayandor@buffalo.edu

7. Copyright Statement

8. Acknowledgements

This project was partly funded by the Academy of Finland postdoctoral project: *From micro-scale data to macro-scale understanding*.

References

[1] Shah, S., Bayandor, J., Abdi, F. and Najafi, A. Micro mechanics based prognosis of progressive dynamic damage in advanced aerospace composite structures. In *27th Congress of the International Council of the Aeronautical Sciences*, Nice, France, 2010.

[2] Bayandor, J., Johnson, A.F., Thomson, R.S., Joosten, M. Impact damage modelling of composite aerospace structures subject to bird-strike. In *25th Congress of the International Council of the Aeronautical Sciences*, Hamburg, Germany, 2006.

[3] Kim, M., Zammit, A. and Bayandor, J. Bird strike damage tolerance analysis of composite turbofan engines, In *27th Congress of the International Council of the Aeronautical Sciences*, Nice, France, 2010.

[4] Orifici, A. C., Thomson, R. S., Degenhardt, R., and Bayandor, J. The design of postbuckling composite aerospace structures accounting for damage initiation and growth. In *26th Congress of International Council of the Aeronautical Sciences*, Anchorage, Alaska, USA, 2008.

[5] Basso, N., Chishti, M., Bayandor, J., Thomson, R., and Bisagni, C. Investigation of adhesively bonded composite structure joints. In *26th Congress of the International Council of the Aeronautical Sciences*, Anchorage, Alaska, USA, 2008.

[6] Horton, B. and Bayandor, J. Numerical investigation of fan-blade out using meso-scale composite modelling. In *30th Congress of the International Council of the Aeronautical Sciences*, Daejeon, Korea, 2016.

[7] LLorca, J. González, C. Molina-Aldareguía, J.M. and Lopes, C. S. Multiscale modeling of composites: toward virtual testing and beyond. *The Journal of The Minerals, Metals & Materials Society*, Vol. 65, No. 2, pp. 215-225, 2013.

[8] Hinton, M. J. Kaddour, A. S. Soden, P.D. Failure Criteria in Fibre-Reinforced-Polymer Composites – The World-Wide Failure Exercise, Edition 1, Elsevier Ltd, 2004.

[9] American Society of Testing and Materials, ASTM D5628-10 Standard Test Method for Impact Resistance of Flat, Rigid Plastic Specimens by Means of a Falling Dart (Tup or Falling Mass), *ASTM International*, 2010.

[10] Kress, G. Examination of Hashin's failure criteria for the second world-wide failure exercise, *Journal of Composite Materials*, Vol. 16, No. 1, pp. 2-19, 1982.

[11] Puck, A. Schürmann, H. Failure analysis of FRP laminates by means of physically based phenomenological models. In *Failure criteria in fibre-reinforced-polymer composites*, Elsevier Ltd, Vol. 62, pp. 1633-1662, 2002.

[12] Cuntze, R.G. Freund, A. The predictive capability of failure mode concept-based strength criteria for multidirectional laminates. In *Failure criteria in fibre-reinforced-polymer composites*, Elsevier Ltd, Vol. 64, No. 3, pp. 343-377, 2004.

[13] Rybicki, E. F. Kanninen, M. F. A finite element calculation of stress intensity factors by a modified crack closure integral, *Engineering fracture mechanics*, Vol. 9, No. 4, pp. 931-938, 1977.

[14] Jokinen, J. Wallin, M. Kanerva, M. Saarela, O. Analyses of criticality for multiple site delamination in the flap spar of Finnish F/A-18 aircraft, *The Aeronautical Journal*, Vol. 125, pp. 556-577, 2020.

[15] *Conference proceedings from the American Society of Composites*, Tenth Technology Proceedings: Composite Materials, Mechanics and Processing on October 18-20, at the Miramar Sheraton Hotel Santa Monica, California, 1995.

[16] Skyttä, V. Saarela, O. Wallin M. Progressive failure of composite laminates; Analysis vs experiments. Laboratory of Lightweight Structures. Helsinki University, 2006.

[17] Hintikka, P. Wallin, M. Saarela, O. The effect of moisture on the interlaminar fracture toughness of CFRP laminate. In *27th Congress of International Council of the Aeronautical Sciences*, Nice, France, 2010.

[18] Chang, F. K. Kuo-Yen, C. A progressive damage model for laminated composites containing stress concentrations. *Journal of composite materials,* Vol. 21, No.9, pp 834-855, (1987).

[19] Hashin, Z. Failure Criteria for Unidirectional Fibre Composites. *Journal of Applied Mechanics*, Vol. 47, pp. 329–334, 1980.

[20] Wade, B. Feraboli, P. Osborne, M. Simulating laminated composites using LS-DYNA material model MAT54 part I: [0] and [90] ply single-element investigation. FAA JAMS. Baltimore, MD, USA, 2012.

[21] Cherniaev, A. Montesano, J. Butcher, C. Modelling the axial crush response of CFRP tubes using MAT054, MAT058 and MAT262 in LS-DYNA. *Proceedings of the 15th International LS-DYNA® Users Conference*, Detroit, MI, USA. 2018.

[22] Hallquist, J. O. LS-DYNA keyword manual volume I & II, Livermore, CA, 2015.

[23] Horton, B. Comprehensive Multi-Scale Progressive Failure Analysis for Damage Arresting Advanced Aerospace Hybrid Structures. Dissertation Virginia Tech, 2017.

[24] Turon, A. Davila, C. G., Camanho, P. P. Costa, J. An engineering solution for mesh size effects in the simulation of delamination using cohesive zone models. *Engineering fracture mechanics*, Vol. 74, No. 10, pp 1665-1682, 2007.

[25] Bak, B. L. Sarrado, C. Turon, A. Costa, J. Delamination under fatigue loads in composite laminates: a review on the observed phenomenology and computational methods. *Applied Mechanics Reviews*, Vol. 66, No. 6, 2014.

[26] ASTM D5528-13, Standard Test Method for Mode I Interlaminar Fracture Toughness of Unidirectional Fibre-Reinforced Polymer Matrix Composites, *ASTM International*, West Conshohocken, PA, 2013.

[27] Benzeggagh, M.L. Kenane, M. Measurement of mixed-mode delamination fracture toughness of unidirectional glass/epoxy composites with mixed-mode bending apparatus. *Composites science and technology*, Vol. 56, pp. 439–449, 1996.

[28] Irwin, GR. Plastic zone near a crack and fracture toughness. *Proceedings of the seventh Sagamore Ordnance materials conference*, New York: Syracuse University, Vol. 4, p. 63–78, 1960.

[29] Hui, C. Y, Jagota, A. Bennison, S. J. Londono, J. D. Crack blunting and the strength of soft elastic solids. *Proceedings of the Royal Society of London. Series A: Mathematical, Physical and Engineering Sciences*, Vol. 459, No. 2034, pp. 1489-1516, 2003.

[30] Dugdale, D. S. Yielding of steel sheets containing slits. *Journal of the Mechanics and Physics of Solids*, Vol. 8, No. 2, pp. 100-104, 1960.

[31] Barenblatt, G. I. The mathematical theory of equilibrium cracks in brittle fracture. *Advances in applied mechanics*. Vol. 7, pp. 55-129, 1962.

[32] Rice, J. R. The mechanics of earthquake rupture. *Proceeding of the international school of physics*, pp. 555–649,

1979.

[33] Falk, Michael L. Needleman, Alan and Rice, James R. A critical evaluation of cohesive zone models of dynamic fractur. *Le Journal de Physique IV*, Vol. 11, No. PR5, pp. Pr5-43, 2001.

[34] Hillerborg, A. Modéer, M. Petersson, P-E. Analysis of crack formation and crack growth in concrete by means of fracture mechanics and finite elements. *Cement and concrete research*, Vol. 6, No. 6, pp. 773-781, 1976.

[35] Song, K. Dávila, C. G. Rose, C. A. Guidelines and parameter selection for the simulation of progressive delamination. *Abaqus User's conference*, Vol. 41, 2008.

[36] Lemmen, P. P. M. Meijer, G. J. Failure prediction tool theory and user manual, *TNO Report*, 2001.

[37] Mohammed, G. Paiva, J. M. F. Mayer, S. Oasys LS-DYNA Environment: Introduction to Composites Modelling in LS-DYNA, 2019.

[38] Siddens, A. Bayandor, J. Multidisciplinary impact damage prognosis methodology for hybrid structural propulsion systems. *Computers & Structures*, Vol. 122, pp. 178-191, 2013.

[39] Bayandor, J. Thomson, R. S. Callus, P. J. Modelling the low velocity impact response of an aerospace composite replacement panel. In *24th Congress of the International Council of the Aeronautical Sciences*, Yokohama, Japan, USA, 2004.

Appendix

The formulation of Hashin's failure criterion for the inter-fibre modes is as follows:

Hashin's criterion

$$IFF_{+} = \frac{(\sigma_{11} + \sigma_{33})^2}{Y_t^2} + \frac{(\sigma_{23}^2 - \sigma_{22}\sigma_{33})}{S_{23}^2} + \frac{(\sigma_{12}^2 + \sigma_{13}^2)}{S_{12}^2} \quad for\ (\sigma_{22} + \sigma_{33}) \geq 0 \tag{1}$$

$$IFF_{-} = \frac{1}{Y_c}\left[\left(\frac{Y_c}{2S_{23}}\right) - 1\right](\sigma_{22} + \sigma_{33}) + \frac{(\sigma_{22} + \sigma_{33})^2}{4S_{23}^2} + \frac{(\sigma_{23}^2 - \sigma_{22}\sigma_{33})}{S_{23}^2} + + \frac{(\sigma_{12}^2 + \sigma_{13}^2)}{S_{12}^2} \quad for\ (\sigma_{22} + \sigma_{33}) < 0 \tag{2}$$

Puck's failure criterion for the inter-fibre modes:

Puck's criterion

$$IFF_{+}(\theta) = \sqrt{\left[\left(\frac{1}{R_{\perp}^{+A}} - \frac{p_{\perp\psi}^{+}}{R_{\perp\psi}^{A}}\right)\sigma_n(\theta)\right]^2 + \left(\frac{\tau_{nt}(\theta)}{R_{\perp\perp}^{A}}\right)^2 + \left(\frac{\tau_{nl}(\theta)}{R_{\perp\parallel}^{A}}\right)^2} + \frac{p_{\perp\psi}^{+}}{R_{\perp\psi}^{A}}\sigma_n(\theta) \quad for \quad \sigma_n(\theta) \geq 0 \tag{3}$$

$$IFF_{-}(\theta) = \sqrt{\left[\left(\frac{p_{\perp\psi}^{-}}{R_{\perp\psi}^{A}}\right)\sigma_n(\theta)\right]^2 + \left(\frac{\tau_{nt}(\theta)}{R_{\perp\perp}^{A}}\right)^2 + \left(\frac{\tau_{nl}(\theta)}{R_{\perp\parallel}^{A}}\right)^2} + \frac{p_{\perp\psi}^{-}}{R_{\perp\psi}^{A}}\sigma_n(\theta) \quad for \quad \sigma_n(\theta) < 0 \tag{4}$$

where,

$$\sigma_n(\theta) = \sigma_{22}\cos^2\theta + \sigma_{33}sin^2\theta + 2\sigma_{23}sin\theta cos\theta \tag{5a}$$

$$\tau_{nt}(\theta) = (\sigma_{33} - \sigma_{22})sin\theta cos\theta + \sigma_{23}(cos^2\theta - sin^2\theta) \tag{5b}$$

$$\tau_{nl}(\theta) = \sigma_{31}\sin\theta + \sigma_{21}cos\theta \tag{5c}$$

with,

$$\frac{p_{\perp\psi}^{+}}{R_{\perp\psi}^{A}} = \frac{p_{\perp\perp}^{+}}{R_{\perp\perp}^{A}}\cos^2\psi + \frac{p_{\perp\parallel}^{+}}{R_{\perp\parallel}^{A}}\sin^2\psi \tag{6a}$$

$$\frac{p_{\perp\psi}^{-}}{R_{\perp\psi}^{A}} = \frac{p_{\perp\perp}^{-}}{R_{\perp\perp}^{A}}\cos^2\psi + \frac{p_{\perp\parallel}^{-}}{R_{\perp\parallel}^{A}}\sin^2\psi \tag{6b}$$

where,

$$\cos^2\psi = \frac{\tau_{nt}^2}{\tau_{nt}^2 + \tau_{nl}^2} \tag{7a}$$

$$\sin^2\psi = \frac{\tau_{nl}^2}{\tau_{nt}^2 + \tau_{nl}^2} \tag{7b}$$

Cuntze's failure criterion for the inter-fibre modes:

Cuntze's criterion models the five different failure modes by a simple probabilistic series as spring models. The criterion describes the lamina's damage as a series of failure systems, which fail whenever any of the modes fail.

Therefore, the interaction between FF and IFF modes are defined using stress effort, which sums up the contribution of each mode.

Cuntze's criterion

$$FF1:\ F_{\parallel}^{\sigma} = \frac{I_1}{\bar{R}_{\parallel}^{t}} \tag{8}$$

$$FF2:\ F_{\parallel}^{\tau} = \frac{-I_1}{\bar{R}_{\parallel}^{c}} \tag{9}$$

$$IFF1:\ F_{\perp}^{\sigma} = \frac{I_2 + \sqrt{4}}{2\bar{R}_{\perp}^{t}} \tag{10}$$

$$IFF2:\ F_{\perp\parallel} = \frac{{I_3}^{3/2}}{\bar{R}_{\perp\parallel}^{3}} + b_{\perp\parallel}\frac{I_2 I_3 - I_5}{\bar{R}_{\perp\parallel}^{3}} \tag{11}$$

$$IFF3:\ F_{\perp}^{\tau} = (b_{\perp}^{\tau} - 1)\frac{I_2}{\bar{R}_{\perp}^{c}} + \frac{b_{\perp}^{\tau} I_4 + b_{\parallel\perp}^{\tau} I_3}{\bar{R}_{\perp}^{c2}} \tag{12}$$

where the invariant components are,

$$I_1 = \sigma_{11} \tag{13a}$$

$$I_2 = \sigma_{22} + \sigma_{33} \tag{13b}$$

$$I_3 = \sigma_{31}^2 + \sigma_{21}^2 \tag{13c}$$

$$I_4 = (\sigma_{22} - \sigma_{33})^2 + 4\sigma_{23}^2 \tag{13d}$$

$$I_5 = (\sigma_{22} - \sigma_{33})(\sigma_{32}^2 - \sigma_{21}^2) - 4\sigma_{23}\sigma_{31}\sigma_{21} \tag{13e}$$

with the function (fitting) parameters of,

$$b_{\perp\parallel} = \frac{1 - \left(\frac{\sigma_{21}^{\perp\parallel}}{\bar{R}_{\perp\parallel}}\right)^2}{\frac{2\sigma_{22}\sigma_{21}^{\perp\parallel 2}}{\bar{R}_{\perp\parallel}^{3}}} \tag{14a}$$

$$b_{\perp}^{\tau} = \frac{1 + \frac{(\sigma_{22} + \sigma_{33})}{\bar{R}_{\perp}^{c}}}{\frac{(\sigma_{22} + \sigma_{33})}{\bar{R}_{\perp}^{c}} + \frac{(\sigma_{22} - \sigma_{33})^2}{\bar{R}_{\perp}^{c2}}} \tag{14b}$$

$$b_{\parallel\perp}^{\tau} = 1 - (b_{\perp}^{\tau} - 1)\frac{\sigma_{21}^{\perp\parallel}}{\bar{R}_{\perp\parallel}} - b_{\perp}^{\tau}\left(\frac{\sigma_{21}^{\perp\parallel}}{\bar{R}_{\perp\parallel}}\right)^2 \tag{14c}$$

The stress effort variable includes:

$$Eff^m = (Eff^{\parallel\sigma})^m + (Eff^{\parallel\tau})^m + (Eff^{\perp\sigma})^m + (Eff^{\perp\tau})^m + (Eff^{\perp\parallel})^m \tag{15}$$

where variable m is the interaction exponent obtained by curve fitting (for CFRP recommended range is 2.5<m<3.5).

The three criteria use the same failure modes for the fibre direction (tension/compression):

$$FF1 = \frac{\sigma_{11}}{X_t} \tag{16a}$$

$$FF2 = \frac{-\sigma_{11}}{X_c} \tag{16b}$$

The tensile fibre mode of the Hashin's criterion is different and as follows:

$$FF1 = \left(\frac{\sigma_{11}}{X_t}\right)^2 + \frac{{\sigma_{12}}^2 + {\sigma_{13}}^2}{{S_{12}}^2} \tag{17}$$

Chang – Chang criterion

The Chang-Chang failure mode is described by the following equations:

Tensile fibre mode:

$$e_f{}^2 = \left(\frac{\sigma_{aa}}{X_t}\right)^2 + \beta\left(\frac{\sigma_{ab}}{S_c}\right)^2 - 1 \qquad \begin{matrix} e_f{}^2 \geq 0 \rightarrow failed \\ e_f{}^2 < 0 \rightarrow elastic \end{matrix} \qquad (18)$$

Compressive fibre mode:

$$e_c{}^2 = \left(\frac{\sigma_{aa}}{X_c}\right)^2 - 1 \qquad \begin{matrix} e_c{}^2 \geq 0 \rightarrow failed \\ e_c{}^2 < 0 \rightarrow elastic \end{matrix} \qquad (19)$$

where *a* represents the fibre direction, *b* and *c* denote the matrix and through-thickness direction. X_t and X_c are the fibre longitudinal tensile and compressive strengths, respectively, and e_f as well as e_c are the fibre failure parameter. σ_{aa} represents the longitudinal stress and σ_{ab} the shear stress of each layer. S_c denotes the matrix shear strength [23].

Tensile matrix mode:

$$e_m{}^2 = \left(\frac{\sigma_{bb}}{Y_t}\right)^2 + \left(\frac{\sigma_{ab}}{S_c}\right)^2 - 1 \qquad \begin{matrix} e_m{}^2 \geq 0 \rightarrow failed \\ e_m{}^2 < 0 \rightarrow elastic \end{matrix} \qquad (20)$$

Compressive matrix mode:

$$e_d{}^2 = \left(\frac{\sigma_{bb}}{2S_c}\right)^2 + \left[\left(\frac{Y_c}{2S_c}\right)^2 - 1\right]\frac{\sigma_{bb}}{Y_c} + \left(\frac{\sigma_{ab}}{S_c}\right)^2 - 1 \qquad \begin{matrix} e_d{}^2 \geq 0 \rightarrow failed \\ e_d{}^2 < 0 \rightarrow elastic \end{matrix} \qquad (21)$$

where Y_t and Y_c are the transverse tensile and compressive strength of the matrix. e_m and e_d are the matrix failure parameter that determines matrix cracking [20].